AIP | Applied Physics Letters

Understanding the deformation mechanism of individual phases of a ZrTi-based bulk metallic glass matrix composite using in situ diffraction and imaging methods

Yongjiang Huang, J. C. Khong, Thomas Connolley, and J. Mi

Citation: Applied Physics Letters **104**, 031912 (2014); doi: 10.1063/1.4863095
View online: http://dx.doi.org/10.1063/1.4863095
View Table of Contents: http://scitation.aip.org/content/aip/journal/apl/104/3?ver=pdfcov
Published by the AIP Publishing

Understanding the deformation mechanism of individual phases of a ZrTi-based bulk metallic glass matrix composite using *in situ* diffraction and imaging methods

Yongjiang Huang,[1,2,a),b)] J. C. Khong,[2] Thomas Connolley,[3] and J. Mi[2,a)]
[1]*School of Materials Science and Engineering, Harbin Institute of Technology, Harbin, China*
[2]*School of Engineering, University of Hull, East Yorkshire, United Kingdom*
[3]*I12 JEEP Beamline, Diamond Light Source, Oxfordshire, United Kingdom*

(Received 20 December 2013; accepted 10 January 2014; published online 24 January 2014)

The plasticity of a ZrTi-based bulk metallic glass composite consisting of glassy matrix and crystalline dendritic phase was studied *in-situ* under identical tensile loading conditions using scanning electron microscopy and synchrotron X-ray diffraction. A generic procedure was developed to separate the diffraction information of the crystalline phases away from that of the matrix and to precisely calculate the microscopic strains of the two phases at different macroscopic load steps. In this way, the time-evolved quantitative links between shear bands nucleation/propagation and the corresponding microscopic stress fields around them are established, providing more quantitative understanding on (1) how the shear bands are driven by the local stress field, and (2) the critical stresses required for the shear bands to nucleate in the crystalline phase, propagate through the crystalline/matrix interface, and finally into the matrix. © *2014 AIP Publishing LLC*.
[http://dx.doi.org/10.1063/1.4863095]

Bulk metallic glasses (BMGs) have been attracting considerable interest because of their high fracture strength, excellent wear and corrosion resistance, and many other promising functional properties.[1] However, they are brittle alloys with limited ductility under compression, and near zero plasticity under tension.[2] To tackle this fundamental problem, researchers have developed several BMG matrix composites (BMGMCs) by fine tuning the chemical compositions or tailoring the microstructures,[3–5] and achieved much improved tensile ductility. Among them, the most promising composites are the *in-situ* cast composites with uniform crystalline phases embedded in the glassy matrix.[6–8] One of the typical examples is the ZrTi-based BMGMCs reported by Hofmann *et al.*[9] with tensile ductility >10% and fracture toughness equal to or higher than steel or Ti alloys. The proposed mechanisms for the increased plasticity are (1) severe lattice distortion and local amorphisation in the crystalline dendrites, (2) the pile-ups of dislocations at the interface between the dendrite and the matrix, and (3) the interface acting as barriers to arrest the rapid propagation of shear bands.[10] Those mechanisms are proposed based mainly on the post-mortem observations of the mechanically tested or fractured samples using scanning electron microscopy (SEM) and/or transmission electron microscopy (TEM). However, most SEM and/or TEM studies were performed on either the fractured samples, or on the tested samples after the mechanical loads was removed. Therefore, the corresponding strain/stress information for the studied samples is missing, and more importantly, the dynamic deformation behaviors of the samples under real-time loadings cannot be revealed. To measure the real-time strain/stress evolution of BMGMCs, synchrotron X-ray diffraction[11–14] has been used. For instance, Ott *et al.*[13] measured the lattice strains around Ta particles in a Zr-based BMGMC during compression, and Suzuki *et al.*[14] studied the compressive deformation behaviors of ZrC particles and glassy matrix. Although considerable progress has been achieved in understanding the fundamental mechanism of the enhanced plasticity of BMGMCs, how the plastic deformation starts in the composite microstructure and at what local stress level have not been reported.

In this letter, we used synchrotron X-ray and SEM to investigate *in-situ* the deformation behaviors of a ZrTi-based BMGMC under identical tensile load conditions and then establish the time-evolved links between the images acquired and the strain/stress field where the images were taken. We also developed a generic procedure to separate the diffraction information of the crystalline phases away from that of the matrix. This allows us to answer quantitatively (1) at what stress, the shear bands are nucleated and (2) at what stress, the shear bands are driven to propagate in the crystalline phase, through the crystalline/ matrix interface, and finally into the matrix.

Alloy ingots with a nominal composition of $Zr_{39.6}Ti_{33.9}Nb_{7.6}Cu_{6.4}Be_{12.5}$ (at. %) were made by arc melting a mixture of Ti, Zr, Nb, Cu, and Be elements with purities higher than 99.9% (wt. %) under a Ti-gettered argon atmosphere. The master alloys were remelted at least four times before casting into a copper mould to form plate-shaped samples of $2 \times 30 \times 40$ mm^3. Dog-bone shaped tensile samples were cut from the as-cast plates (Fig. 1(a)), and carefully ground and polished to 1 μm diamond suspension and 0.025 μm colloidal silica. Fig. 1(b) shows the typical as-cast microstructure with dendritic crystalline phases (2–6 μm in size and a volume fraction of 59.5%) uniformly distributed within a featureless glassy matrix. Nanoindentation tests (a maximum depth of

a)Authors to whom correspondence should be addressed. Electronic addresses: j.mi@hull.ac.uk and yjhuang@hit.edu.cn.
b)UK Royal Society K.C. Wong Fellow hosted at University of Hull.

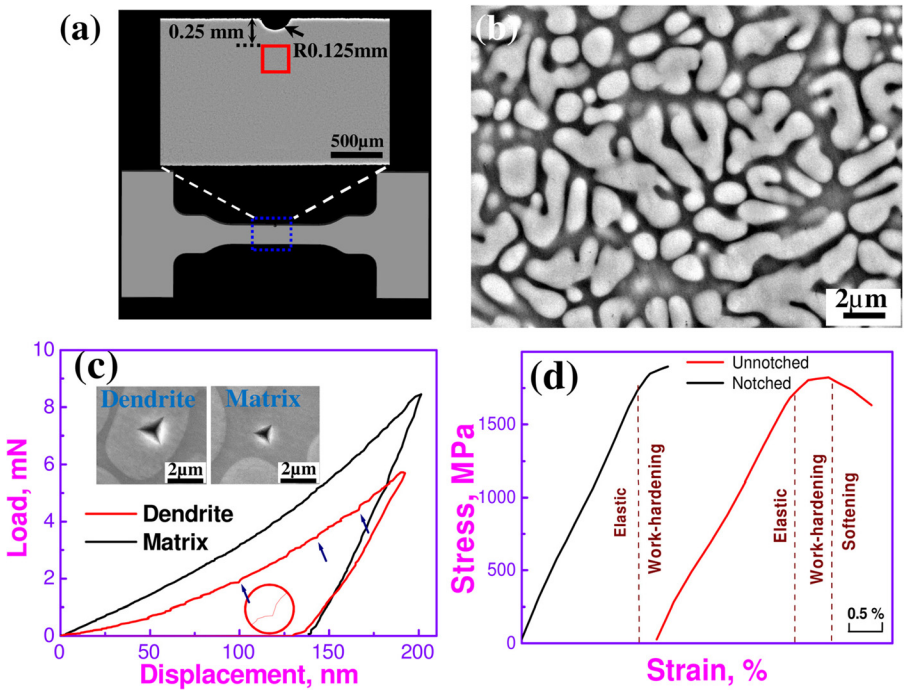

FIG. 1. (a) A dog-bone shaped sample, its dimension, and an inset showing a semi-circular notch in the middle of the gauge length of the sample. The 0.25×0.25 mm^2 square box shows the location where the X-ray diffraction patterns are acquired, (b) a backscattered electron image showing the microstructure of the as-cast composite, consisting of dendrites and matrix; (c) the load-displacement curves obtained from the nanoindentation tests of the dendrites and the matrix, and the residual indents remained on a dendrite and matrix after tests; and (d) the tensile stress-strain curves for the composite samples with and without notch.

200 nm at a strain rate of 0.1 s^{-1}) were performed on the dendrites and the matrix, respectively, using a MTS Indenter with a Berkovich diamond tip. Fig. 1(c) presents the typical load-displacement (*P-h*) curves and the indentation marks on the dendrites and the matrix. The indentation curve for the matrix is very smooth, whereas several pop-in events (marked by arrows and highlighted by a circle in Fig. 1(c)), were found for the dendrites, indicating that shear banding events occurred during indentation. The Oliver-Pharr method[15] was used to determine the nanohardness and Young's modulus of the dendrites (3.12 GPa and 90.91 GPa), and matrix (7.12 GPa and 117.77 GPa), respectively.

For some samples, a semi-circular notch with a diameter of 250 μm (Fig. 1(a)) was cut at one edge in the middle of the gauge length to initiate stress concentration at the notch to facilitate the nucleation and propagation of shear bands. Uniaxial tensile loads were applied stepwise to the samples using a micromechanical stress module, Deben Microtest 2000. X-ray diffraction patterns at the sample location as marked by a square box in Fig. 1(a) at different loads were acquired at the beamline I12 of Diamond Light Source, UK. A monochromatic X-ray beam (98.856 keV, 0.25×0.25 mm^2 beam size) and a Pixium RF4343 two-dimensional (2-D) detector (2880×2881 pixel) were used to record the diffraction patterns at 4 seconds per pattern. The sample-detector distance was set at 472.85 mm to acquire higher Q value up to 20 Å^{-1} ($Q = 4\pi \sin\theta/\lambda$). The detailed X-ray diffraction procedure can be also found in Ref. 12. *In-situ* imaging studies under the identical loading conditions were also performed using the same Microtest inside a Zeiss Evo60 SEM operated at 20 keV.

Fig. 1(d) shows the stress-strain curves for the samples with and without notch. For the unnotched sample, the deformation behavior is characterized by three regions, i.e., elastic, work hardening, and softening regions. However, for the notched sample, just a very narrow work hardening region appeared on the stress-strain curve above the elastic limit. The notch, as a stress concentrator, can initiate shear bands locally, and because the stress decreases exponentially away from the notch, the propagation of the nucleated shear bands can be controlled in a steady-state manner at different load steps.[12] In this way, we can effectively "hold" the shear band in place at a particular load level, imaging the shear bands using SEM and acquiring X-ray diffraction patterns at the location near the shear bands and later to precisely calculate the local strains. By combining the *in-situ* imaging and diffraction studies together, the link between the local strain/stress field and the shear band characteristics was investigated in real time, providing more quantitative understanding on the deformation mechanism of BMGMCs.

Fig. 2(a) shows a typical diffraction pattern of the as-cast composite. Discrete diffraction spots from the dendrites appear and superimpose on the diffuse diffraction rings from the matrix. Because of this coupled nature, to separate the diffracted intensity of the dendrites completely away from that of the matrix is very challenging. Although several attempts concerning this aspect had been made,[7,13,14] they all used a specific method to deal with a special case, or patterns. For instance, Qiao *et al.*[7] manually selected sectors in the azimuthal direction from the 2-D diffraction rings, and the angle of each sector was chosen differently to avoid any diffracted spots from the crystalline dendrites in that sector. By integrating the 2-D diffraction information in each sector into a 1-D curve and then "stitching" each curve together, a 1-D diffraction spectrum for the matrix is constructed. Apparently, this manual approach assumes that the 2-D diffraction information from the matrix is homogenous and azimuthal-angle independent. However, when a sample is subject to an external load, the 2-D diffraction rings contain azimuthal-angle dependent deformation information, as reported by Stoica *et al.*[16] and Qu *et al.*[17] Hence, the method reported in Ref. 7 is not suitable for calculating the strains of composites under an external load. While in Refs. 13 and 14, the diffraction peaks from the reinforcing particles do not have strong coupling with the matrix diffraction halo,

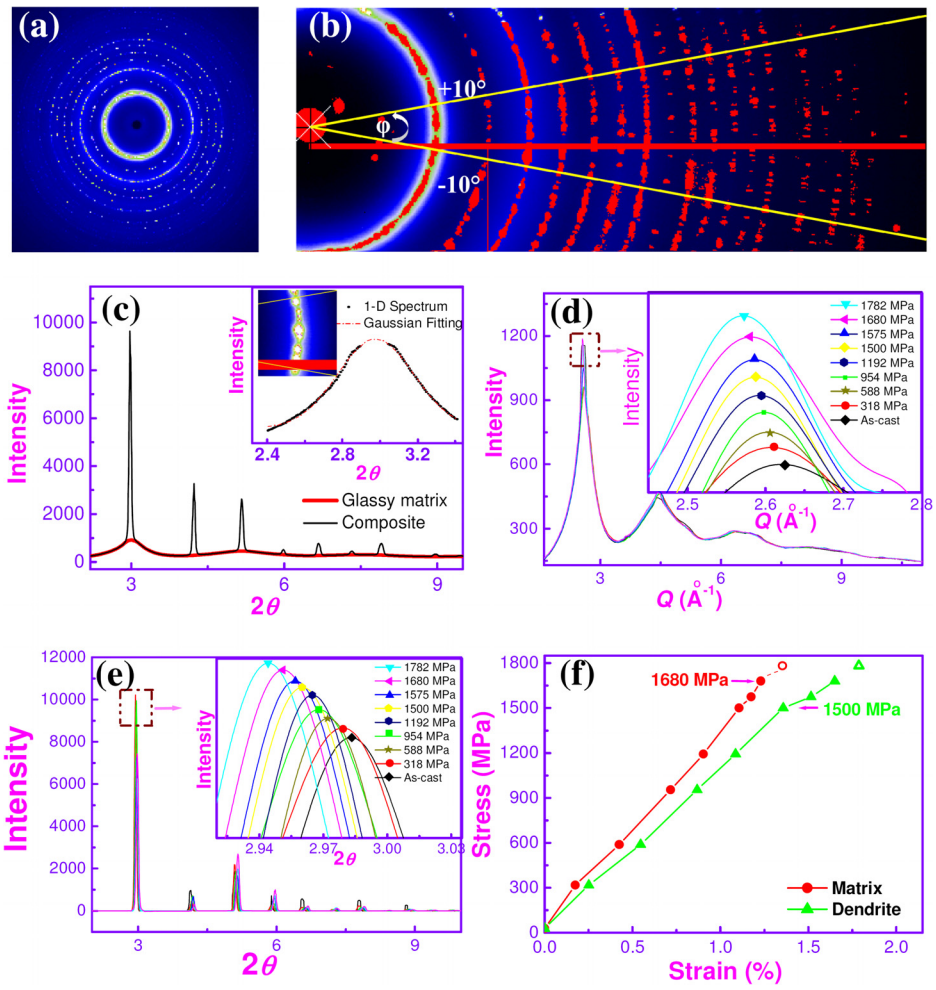

FIG. 2. (a) A typical X-ray diffraction pattern for the as-cast ZrTi composite, (b) an enlarged section of the composite diffraction pattern, highlighting the diffractin rings and the spots, (c) the 1-D X-ray intensity curve of the composite and that of the matrix separated, (d) the 1-D X-ray intensity curve, $I(Q)$, for the glassy matrix, and (e) those for the crystalline dendrites at different stress levels with the insets showing the shifts of the 1st peaks, and (f) the calculated strains for the glassy matrix and the crystalline dendrites at different stress levels along tensile direction. In order to get a much clearer strain-stress relationship, the strains at 1782 MPa for the matrix and the dendrite are also estimated using the same method, and presented in Fig. 2(f).

and therefore decoupling was not performed. A generic procedure or algorithm that can be applied generally to the acquired diffraction patterns to separate the diffraction data of the crystalline phases away from that of the matrix has not been reported until now. We therefore develop an iterative and generic procedure to completely mask out the discrete diffraction spots using Fit2D[18] during the integration of the 2-D ring into a 1-D spectrum. First, the X-ray diffraction rings of the composite acquired at different loads were segmented anticlockwise into 9 parts (20° sector for each part) in the azimuthal φ range of 0 to π using Fit2D, and one part in the tensile loading directions ($\varphi = 0°$) is shown in Fig. 2(b). Second, a search step of 0.01 Å^{-1} is defined in the Q range from 0 to 20 Å^{-1}, at each Q step, a Fit2D algorithm is used to calculate the average intensity, then any intensity 10% higher than this average value is considered as the diffraction information from the crystalline phases, and therefore masked out. After the first masking out, the average diffraction intensity along the same arc is re-calculated, and any intensity 10% higher than the newly average value is again masked out. This procedure is carried out iteratively until no intensity within the searched arc is 10% higher than the average value calculated at the current search. In this way, the crystalline diffraction spots that have sufficient distance can be completely masked out. However, for those crystalline diffraction spots that are nearly touching with each other like those shown in Fig. 2(c) inset, when the diffraction intensity is taken out, there will be a void in the Q space, typically in a small range of 0.05–0.1 Å^{-1}. We use Gaussian fitting to recover the missing data for those cases. Using the above procedure, the diffraction information of the matrix is completely separated from the composite diffraction rings. The separated 2-D diffuse diffraction halo is then integrated to form a 1-D intensity spectrum using[16]

$$I_i(Q, \varphi_I) = \int_{\varphi-\pi/9}^{\varphi+\pi/9} [I(Q, \varphi) + I(Q, \varphi + \pi)] d\varphi \qquad (1)$$

with $i = 1....9$, where $Q = Q(s)$ is defined as,[16]

$$Q(s) = \frac{4\pi}{\lambda} \sin[\arctan(s/D)/2], \qquad (2)$$

where λ is the X-ray wavelength, D is the sample-to-detector distance, and s is the distance from the origin of the polar coordinate system. Fig. 2(c) shows $I(Q)$ curves for the as-cast composite and the matrix separated.

When subjected to different loads, the relative shifts of the positions of the first peaks of $I(Q)$ curves obtained at each load-step (Fig. 2(d)) were used to calculate the elastic strains

$$\varepsilon_Q = \frac{Q - Q_0}{Q_0}, \qquad (3)$$

where Q and Q_0 represent the first peak positions of $I(Q)$ curves at σ and zero stress, respectively.

For the crystalline dendrites, their diffraction intensity curves can be simply obtained by subtracting the decoupled glassy matrix diffraction intensity away from that of the composite. The first peak positions in the intensity curves were obtained (Fig. 2(e) inset) using Gaussian fitting, and the strain was calculated based on the peak shift using

$$\varepsilon_D = \frac{I_{2\theta,\sigma} - I_{2\theta,0}}{I_{2\theta,0}}, \tag{4}$$

where $I_{2\theta,\sigma}$ and $I_{2\theta,0}$ represent the first peak positions at σ and zero stress, respectively.

Figs. 2(d) and 2(e) show the shifts of the intensity curves of the matrix and the dendrites at different stresses, respectively. The corresponding insets show that, as the stresses increase, the peaks shift to smaller values. The stress-strain relationships were plotted in Fig. 2(f). Initially, both matrix and dendrites exhibit linear stress-strain relationship. No shear band can be found as typically shown in Fig. 3(a) at 588 MPa. As the stress increased to 1500 MPa, a few shear bands of $\sim$10 μm long were found on the dendrites (Fig. 3(b)), indicating the onset of plastic deformation inside the dendrites, but the matrix remained elastic because no shear band was found in the matrix. Those shear bands in the dendrites were found to "cut" through the dendrites and propagate into the matrix as the stress increased to 1680 MPa (Fig. 3(c)), triggering the plastic deformation of the matrix. Fig. 3(c) clearly shows that those shorter shear bands shown in Fig. 3(b) now grew to 40–50 μm in length, and Fig. 3(c) inset shows that across the dendrite-matrix interface, the shear band is no longer a straight line, and it changes direction when passing across the interface. Fig. 3(d) shows that, when the stress increases further to 1782 MPa, tens of shear bands of many hundreds of micrometers in length appear on the sample surface with coalescence voids observed along an individual shear band (point A), at the dendrite-matrix interface (point B) and on the matrix (point C). Clearly, at this stress level, macroscopically plastic deformation occurs in both dendrites and glassy matrix. After this point, widespread plastic deformation was observed on the composite, and the sample failed with the soft dendrites seriously distorted. Apparently, after the macroscopically plastic deformation occurs as demonstrated in Fig. 3(d), the plastic component of the strain associated with the plastic deformation cannot be revealed by using the peak shifts methods from the diffraction data, and therefore our strain calculation was made to 1680 MPa where only a few shear bands were found, i.e., the point of the start of the plastic deformation. Fig. 2(f) shows that, for the dendrites, the linear stress-strain relationship starts to break away at 1500 MPa when a few shear bands were observed inside them, while for the matrix, the break-away starts at 1680 MPa when shear bands were found to pass across the dendrite-matrix interface and into the matrix. Hence, the stress thresholds at which the dendrite and the matrix start to deform plastically were obtained, using the complementary *in-situ* imaging and diffraction techniques.

Generally, monolithic BMG experiences shear localization when subjected to compression or tension loads, resulting in limited plastic deformation capacity.[19–21] For this reason, extensive efforts have been devoted to develop two-phase composites consisting of ductile crystalline phases in a glassy matrix.[22,23] There are two general principles to toughen a brittle matrix through either (1) crack bridging by adding a soft second phase with a strong interface[24] or (2) crack deflecting by adding a strong and hard phase with a weak interface.[25] In this composite, the crystalline dendrites are relatively soft and ductile as confirmed by the nanoindentation tests (Fig. 1(c)). This soft nature allows the dendrites to deform plastically first at 1500 MPa (Figs. 2(f) and 3(b)), and most nucleated shear bands were confined within the domains having a spatial scale of the order of the dendrite axe length. While the working hardening resulted from the

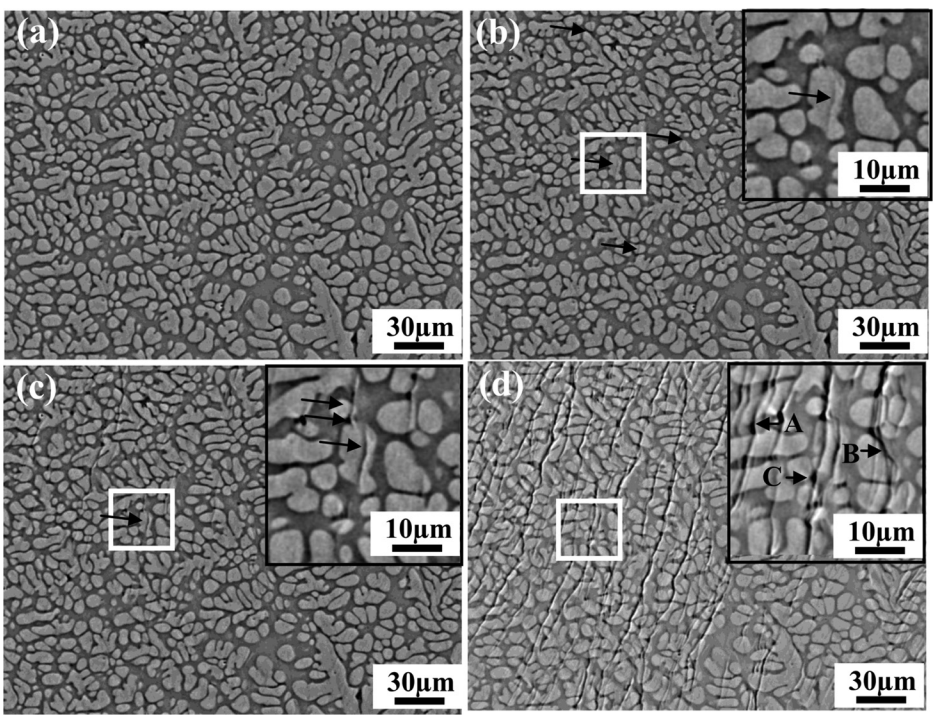

FIG. 3. The backscattered scanning electron images, showing the microstructure, and the shear band nucleation and propagation at the location where the diffraction patterns are acquired at different stress levels of: (a) 588 MPa, (b) 1500 MPa, (c) 1680 MPa, and (d) 1782 MPa. For (b), (c), and (d), the insets show the enlarged images of the rectangular areas.

dislocations inside the dendrites are also demonstrated in the very narrowed work hardening region shown in Fig. 1(d). This effectively increases the plasticity of the composite. Additionally, the dendrites were formed *in situ* during solidification, the bonding strength of the dendrite-matrix interface is naturally stronger than those made by other methods, i.e., powder metallurgy. This strong interface is able to effectively deflect or arrest the fast propagation of shear bands, as shown in Fig. 3(c) inset where the shear bands change the propagation orientation across the interface. Hence, more energy (stress) is needed for the shear bands to propagate in a highly zig-zag manner as shown in Fig. 3(d), resulting in the enhanced plasticity and strength of the composite. However, at the later stage of plastic deformation, when many nearly parallel shear bands form and pass through the dendrite network collectively, the interfaces cannot deflect the collective movement of the shear band clusters, work softening occurs and the sample fails as the shear bands quickly propagate through the sample.

In summary, the tensile deformation of a ZrTi-based bulk metallic glass matrix composite has been studied *in-situ* using synchrotron X-ray diffraction and electron imaging. A generic procedure is developed to separate the diffraction information of the crystalline dendrites away from that of the matrix. Using this method, the stresses at which the dendrites and the glassy matrix start to deform plastically are quantitatively determined at 1500 MPa and 1680 MPa, respectively, and are confirmed by the *in situ* SEM observations of the shear band formation at those stress levels.

The authors (Y. J. Huang and J. Mi) are very grateful for the financial support from the U.K. Royal Society K.C. Wong Fellowship and Diamond Light Source for allocating beam time under the proposal No. EE7665. Y. J. Huang would also like to acknowledge the financial support from the National Natural Science Foundation of China under Grant Nos. 51371065 and 50904021, the Fundamental Research Funds for the Central Universities under Grant No. HIT. NSRIF. 2012001, Postdoctoral Science-Research Developmental Foundation of Heilongjiang Province under Grant No. LBH-Q12073, and the Science and Technology Innovation Talents Special Fund of Harbin under Grant No. 2012RFQXS066.

[1]W. Klement, R. H. Willens, and P. Duwez, Nature **187**, 869 (1960).
[2]A. L. Greer, Science **267**, 1947 (1995).
[3]S. Pauly, S. Gorantla, G. Wang, U. Kühn, and J. Eckert, Nature Mater. **9**, 473 (2010).
[4]Y. Wu, D. Q. Zhou, W. L. Song, H. Wang, Z. Y. Zhang, D. Ma, X. L. Wang, and Z. P. Lu, Phys. Rev. Lett. **109**, 245506 (2012).
[5]Z. Q. Liu, R. Li, G. Liu, W. H. Su, H. Wang, Y. Li, M. J. Shi, X. K. Luo, G. J. Wu, and T. Zhang, Acta Mater. **60**, 3128 (2012).
[6]J. W. Qiao, A. C. Sun, E. W. Huang, Y. Zhang, P. K. Liaw, and C. P. Chuang, Acta Mater. **59**, 4126 (2011).
[7]J. W. Qiao, E. W. Huang, F. Jiang, T. Ungár, G. Csiszár, L. Li, Y. Ren, P. K. Liaw, and Y. Zhang, Appl. Phys. Lett. **97**, 171910 (2010).
[8]C. C. Hays, C. P. Kim, and W. L. Johnson, Phys. Rev. Lett. **84**, 2901 (2000).
[9]D. C. Hofmann, J.-Y. Suh, A. Wiest, G. Duan, M.-L. Lind, M. D. Demetriou, and W. L. Johnson, Nature (London). **451**, 1085 (2008).
[10]J. W. Qiao, Y. Zhang, P. K. Liaw, and G. L. Chen, Scr. Mater. **61**, 1087 (2009).
[11]H. F. Poulsen, J. A. Wert, J. Neuefeind, V. Honkimaki, and M. Daymond, Nature Mater. **4**, 33 (2005).
[12]Y. J. Huang, J. C. Khong, T. Connolley, and J. Mi, Scr. Mater. **69**, 207 (2013).
[13]R. T. Ott, F. Sansoz, J. F. Molinari, J. Almer, K. T. Ramesh, and T. C. Hufnagel, Acta Mater. **53**, 1883 (2005).
[14]H. Suzuki, J. Saida, T. Shobu, J. Katsuyama, H. Kato, M. Imafuku, and S. Sato, Scr. Mater. **66**, 801 (2012).
[15]W. C. Oliver and G. M. Pharr, J. Mater. Res. **7**, 1564 (1992).
[16]M. Stoica, J. Das, J. Bednarcik, H. Franz, N. Mattern, W. H. Wang, and J. Eckert, J. Appl. Phys. **104**, 013522 (2008).
[17]D. D. Qu, K. D. Liss, Y. J. Sun, M. Reid, J. D. Almer, K. Yan, Y. B. Wang, X. Z. Liao, and J. Shen, Acta Mater. **61**, 321 (2013).
[18]A. P. Hammersley, S. O. Svensson, M. Hanfland, A. N. Fitch, and D. Häusermann, High Press. Res. **14**, 235 (1996).
[19]J. R. Greer and J. T. M. De Hosson, Prog. Mater. Sci. **56**, 654 (2011).
[20]Y. J. Huang, F. L. He, H. B. Fan, and J. Shen, Scr. Mater. **67**, 661 (2012).
[21]Y. J. Huang, J. Shen, and J. F. Sun, Appl. Phys. Lett. **90**, 081919 (2007).
[22]F. F. Wu, S. T. Li, G. A. Zhang, X. F. Wu, and P. Lin, Appl. Phys. Lett. **103**, 151910 (2013).
[23]J. W. Qiao, T. Zhang, F. Q. Yang, P. K. Liaw, S. Pauly, and B. S. Xu, Sci. Rep. **3**, 2816 (2013).
[24]S. F. Guo, L. Liu, N. Li, and Y. Li, Scr. Mater. **62**, 329 (2010).
[25]J. B. Li, J. S. C. Jang, C. Li, S. R. Jian, P. H. Tsai, J. D. Hwang, J. C. Huang, and T. G. Nieh, Mater. Sci. Eng., A **551**, 249 (2012).